

AD-A046 821

ROME AIR DEVELOPMENT CENTER HANSCOM AFB MASS DEPUTY--ETC F/6 9/5  
MATERIAL CHOICE FOR OPTIMUM SAW DEVICE PERFORMANCE.(U)  
NOV 77 R M O'CONNELL, A J SLOBODNIK, P H CARR

UNCLASSIFIED

ETR-77-0034

NL

1 OF 1  
AD  
A046821



14 ETR-77-0034

12 18p

11

2-1-1

AD A 0 46821

6

MATERIAL CHOICE FOR OPTIMUM SAW DEVICE PERFORMANCE

9 B.S.

10

Robert M. O'Connell, Andrew J. Slobodnik, Jr., Paul H. Carr  
Deputy for Electronic Technology (RADC/AFSC)  
Hanscom AFB, Massachusetts 01731

Interim report

11

22 Nov 77

16 2345

19 35

ABSTRACT

The theory of surface acoustic wave propagation is reviewed and some of the various material design parameters which follow from that theory and which must be considered in making the optimum SAW device substrate choice are discussed. The parameters covered include SAW velocity, piezoelectric coupling constant, electromechanical power flow angle, temperature sensitivity, propagation losses, and beam steering and diffraction. Depending upon the device being designed and the application, some of these parameters are more important than others. In the design of temperature stable, broadband, low insertion loss devices, the important requirements are a zero temperature coefficient of time delay and a large piezoelectric coupling constant. Alternatively, the design of high frequency devices requires low loss substrate materials with large SAW velocities. The state-of-the-art in the development of new materials for these two classes of devices is reviewed.

1. INTRODUCTION

Because of their small size and low cost, surface acoustic wave (SAW) devices are becoming increasingly attractive for many applications (IEEE Proceedings, 1976). Fundamental to the optimum design of a SAW device is the proper choice of substrate material. A wise decision concerning this choice requires an understanding of the various material factors and tradeoffs inherent in the design of a SAW device. These elements will be discussed in an attempt to provide useful guidelines for the design of SAW devices up to microwave frequencies. The paper will begin with a brief outline of the theory of SAW propagation and the four important factors which describe it. These include SAW velocity, piezoelectric coupling constant, electromechanical power flow angle, and temperature coefficient of time delay. This will be followed by a discussion of various sources of material-related insertion loss, including propagation losses and beam steering and diffraction. The manner in which these concepts are applied depends upon the specific application at hand. To demonstrate this, the remainder of the paper will describe the application of these guidelines in materials related efforts to improve two classes of SAW devices: (1) temperature stable, broad-band, low insertion loss devices, and (2) high frequency devices.

One of the major sources of overall device insertion loss at microwave frequencies is propagation loss or attenuation. Not only is the magnitude of this phenomenon important for predicting absolute insertion loss and dynamic range, but its frequency dependence is equally important when, for example, designing filters having particular bandpass characteristics. The experimentally determined magnitude and frequency dependence of loss for several important surface wave materials will be presented.

The combined effects of beam steering and diffraction are also important. Diffraction causes the acoustic beam to lose its rectangular shape while beam steering results in the beam being offset from the desired location (the output transducer). Both contribute to device insertion loss in a manner which is not simply the sum of the separate constituents. Thus, in the general case, design curves must be more specific than the universal information possible when each loss mechanism is considered individually. A quantitative measure of the extent of both beam steering and diffraction is provided by the slope of the power flow angle. A value of zero for this parameter implies isotropic diffraction and no beam steering, while a value of -1 implies minimum diffraction with increased beam steering. These ideas will be discussed in detail.

The design of a broad-band, low insertion loss SAW device with temperature independent performance characteristics requires a substrate material having large piezoelectric coupling and zero temperature coefficient of time delay. Presently, the most readily available SAW substrate materials are lithium niobate and quartz. As can be seen in Fig. 1, lithium niobate has very large piezoelectric coupling ( $\Delta v/v$ ), which is essential for broad-bandwidth and low insertion loss. However, it also has a large temperature coefficient of time delay, which necessitates the use of ovens and other schemes for temperature control. The ST-cut of quartz (Schulz, M.B., ... 1970), on the other hand, is temperature compensated, but it has only 1/40th the piezoelectric coupling of lithium niobate, a definite disadvantage for low insertion loss devices. Consequently, recent developments in the search for temperature compensated materials having piezoelectric coupling greater than that of quartz are of interest and will be discussed.

Currently the upper frequency limit of optically fabricated SAW devices operating at a fundamental mode is about 1 GHz. The design of higher frequency devices requires either electron beam fabrication, advances in the state-of-the-art of optical lithography (Budreau, A.J., ... 1975), or new substrate materials whose SAW velocities are larger than those of either quartz or lithium niobate, both of which are about 3000 m/sec. Certain materials like aluminum nitride, with SAW velocities of about 6000 m/sec, can extend the frequency limit of SAW devices to 2 GHz. Progress in obtaining reproducible thin films of aluminum nitride will be summarized.

2. SURFACE ACOUSTIC WAVE PROPERTIES

2.1 SAW Propagation Theory

The concept of the generation and propagation of a surface acoustic or Rayleigh wave (Rayleigh, Lord, 1885) is depicted in Fig. 2. The electromagnetic signal is converted to an acoustic wave at the input interdigital transducer (IDT) (White, R.M., ... 1965) by means of the piezoelectric effect. The delayed acoustic wave is then converted back to an electromagnetic signal at the output IDT. The energy of the SAW decays exponentially into the material and is generally confined to within a few acoustic wavelengths of the surface.

1473

409 761

DISTRIBUTION STATEMENT A  
Approved for public release;  
Distribution Unlimited

1B

AD No. UDC FILE COPY

A quantitative description of this process requires solution of the problem of acoustic wave propagation on an arbitrary anisotropic piezoelectric medium. That problem has been solved (Campbell, J.J., ... 1968) (Jones, W.R., ... 1969), and an outline of the solution follows. The coordinate system used to define the problem is shown in Fig. 3. The thin conducting plane shown is used to calculate an estimate of the piezoelectric coupling constant, as will be discussed further in the next section.

The solution to the problem is obtained by solving the continuum equations of motion together with Maxwell's equations under the quasi-static assumption, the strain-mechanical displacement relations, the piezoelectric constitutive relations, and the appropriate boundary conditions. When the linear equations describing these quantities (Tiersten, H.F., 1963) (Slobodnik, A.J., Jr., 1976) are combined, the following differential equations for the components of mechanical displacement  $u_i$  and the electric potential  $\varphi$  within the crystalline medium are obtained:

$$\left. \begin{aligned} c'_{ijkl} u_{k,li} + e'_{kij} \varphi_{,ki} &= \rho \ddot{u}_j, \quad j = 1, 2, 3 \\ e'_{ikl} u_{k,li} - \epsilon'_{ik} \varphi_{,ki} &= 0 \end{aligned} \right\} x_3 > 0 \quad (1)$$

$$e'_{ikl} u_{k,li} - \epsilon'_{ik} \varphi_{,ki} = 0 \quad (2)$$

Outside the crystalline medium, Laplace's equation describes the electric potential.

$$\nabla^2 \varphi = 0, \quad -h \leq x_3 \leq 0 \quad (3)$$

In equations (1) and (2), the primed quantities are the elastic constants ( $c'_{ijkl}$ ), the piezoelectric constants ( $e'_{kij}$ ), and the dielectric constants ( $\epsilon'_{ik}$ ) in a rotated coordinate system obtained through the Euler transformation matrix (Goldstein, 1950) in which wave propagation is always along the 1 direction. Note that the summation convention (over 1, 2, 3) for repeated indices is employed. Also, the dot notation refers to differentiation with respect to time, while an index preceded by a comma denotes differentiation with respect to a space coordinate.

Solutions of equations (1) and (2) are assumed to be of the standard complex traveling-wave form in which  $v_s$  is the wave velocity,  $\alpha$  the exponential decay into the crystal, and  $\omega$  the steady-state angular frequency.

$$u_i = \beta_i \exp[-\alpha \omega x_3 / v_s] \exp[j\omega(t - x_1 / v_s)], \quad i = 1, 2, 3 \quad (4)$$

$$\varphi = \beta_4 \exp[-\alpha \omega x_3 / v_s] \exp[j\omega(t - x_1 / v_s)]. \quad (5)$$

The displacements and potentials are considered to be independent of the  $x_2$  coordinate.

Substituting (4) and (5) into (1) and (2) yields a linear homogeneous system of four equations in the unknowns  $\beta_1, \beta_2, \beta_3$  and  $\beta_4$ . The determinant of the coefficients of the unknowns in these equations must be zero in order that a nontrivial solution exist, i.e.,

$$A_8 \alpha^8 + j A_7 \alpha^7 + A_6 \alpha^6 + j A_5 \alpha^5 + A_4 \alpha^4 + j A_3 \alpha^3 + A_2 \alpha^2 + j A_1 \alpha + A_0 = 0 \quad (6)$$

where the coefficients  $A_n, n = 0, 1, \dots, 8$ , are purely real and a particular value of  $v_s$  has been assumed. Since the fields must be bounded, or go to zero as  $x_3 \rightarrow \infty$ , only the roots with nonnegative real parts are allowed. In addition, these roots are either pure imaginary or occur in pairs with positive and negative real parts. In general, roots occur such that four (three for nonpiezoelectric crystals) with positive real parts can be selected. However, if for a given velocity four such roots cannot be found the possibility of degenerate surface waves must be pursued. Upon obtaining the admissible values of  $\alpha$  from equation (6), corresponding values of  $\beta_i$  (to within a constant factor) can be found for each  $\alpha$  from the linear homogeneous system cited above.

The total fields (mechanical displacement and potential) may now be expressed as a linear combination of the fields associated with the admissible values of  $\alpha$ . For  $x_3 > 0$

$$u_i = \sum_{l=1}^4 B^{(l)} \beta_i^{(l)} \exp[-\alpha^{(l)} \omega x_3 / v_s] \exp[j\omega(t - x_1 / v_s)], \quad i = 1, 2, 3 \quad (7)$$

$$\varphi = \sum_{l=1}^4 B^{(l)} \beta_4^{(l)} \exp[-\alpha^{(l)} \omega x_3 / v_s] \exp[j\omega(t - x_1 / v_s)]. \quad (8)$$

In the region  $-h \leq x_3 \leq 0$ , the potential is a solution of Laplace's equation (3). A solution satisfying the continuity condition at  $x_3 = 0$  and vanishing at  $x_3 = -h$  is

$$\varphi = \sum_{l=1}^4 B^{(l)} \beta_4^{(l)} \operatorname{csch}\left(\frac{\omega h}{v_s}\right) \sinh\left(\frac{\omega}{v_s}(x_3 + h)\right) \exp[j\omega(t - x_1 / v_s)], \quad -h \leq x_3 \leq 0. \quad (9)$$

Mechanical and electrical boundary conditions (Campbell, J.J., ... 1968) (Jones, W.R., ... 1969) must also be satisfied by substituting the waveforms of equations (7) to (9) into the appropriate expressions for these conditions. This yields a set of homogenous equations for the so-called partial field amplitudes  $B^{(l)}$ . The transcendental equation obtained by setting the determinant of the matrix of coefficients of this system equal to zero determines the surface-wave velocities for a given set of  $\alpha^{(l)}$ .

Once equation (6) and the set of  $B^{(l)}$  equations have been simultaneously solved by computer iterative techniques (Jones, W.R., ... 1969) for the actual set of  $\alpha^{(l)}$  (with associated  $\beta_i^{(l)}$ ) and the actual surface wave velocity, the partial field amplitudes  $B^{(l)}, l = 1, 2, 3, 4$  may be calculated to within a constant factor.

These amplitudes are used directly to evaluate the components of the mechanical displacement of equation (7) and the electric potential of equation (8). The components of the electric field, strain, electric displacement, and stress as functions of  $\omega x_3$  follow from Maxwell's equations, the strain mechanical

displacement relations, and the piezoelectric constitutive relations, respectively (Tiersten, H.F., 1963) (Slobodnik, A.J., Jr., 1976). Finally, the components of total time average electromechanical power flow are given by

$$\text{Time Average Power} = -\frac{1}{2} \int_0^\infty \text{Re} [T_{ij} \dot{u}_j^*] dx_3 + \frac{1}{2} \int_0^\infty \text{Re} [\dot{\phi}_1^*] dx_3 \quad (10)$$

where the two terms are, respectively, the total complex mechanical and electrical power components.

## 2.2 Major Material Factors

The expressions derived above have been written into a computer program (Campbell, J.J., ... 1968) (Jones, W.R., ... 1969) which has been used extensively to study the SAW properties of many materials (Slobodnik, A.J., Jr., ... 1973a). Using that program it is possible to calculate three of the four material factors of interest in this paper: surface acoustic wave velocity, piezoelectric coupling constant, and electro-mechanical power flow angle.

Beside being necessary in the calculation of the temperature coefficient of time delay, as shown below, the SAW velocity influences the choice of substrate material depending upon the application. For delay lines and other devices requiring large time delays and small package size, low velocity materials are attractive. On the other hand, for high frequency devices, high velocity materials are useful for reducing fabrication resolution requirements (Hartmann, C.S., ... 1975).

The piezoelectric coupling constant  $\Delta v/v$  is defined (Campbell, J.J., ... 1968) for piezoelectric materials as the percentage difference in velocity between free surfaces ( $wh = \infty$ ) and surfaces coated with an infinitesimally thin perfect conductor ( $wh = 0$ ). The validity of this definition as an estimate of the surface wave coupling to an interdigital transducer has been demonstrated several times both experimentally (Collins, J.H., ... 1968) (Schulz, M.B., ... 1972) and theoretically (Ingebrigtsen, K.A., 1969) (Coquin, G.A., ... 1967). Note that for the purposes of this paper piezoelectric coupling is described directly in terms of  $\Delta v/v$  and not the  $K^2$  coupling parameter. Coupling information is of utmost importance in the design of broad-band, low insertion loss devices. It has been shown that for a given maximum allowable amount of insertion loss, the maximum attainable fractional bandwidth is proportional to the square root of the coupling constant (Hartmann, C.S., ... 1975). Hence, because the coupling of lithium niobate is about forty times as large as that of quartz (See Fig.1), devices on lithium niobate have about six times the fractional bandwidth as devices on quartz, for the same amount of insertion loss (Hays, R.M., ... 1976). This explains the popularity of lithium niobate for broad-band applications.

The power flow angle  $\phi$  is defined in Fig. 4 as the angle between the time average electromechanical power flow vector and the direction of propagation (phase velocity vector). Unless  $\phi$  identically equals zero (defined as a pure-mode axis), the condition of beam steering is said to occur. The slope of the power flow angle, that is  $\partial\phi/\partial\theta$ , is a highly important quantity. Its magnitude determines the amount of beam steering resulting from a given unintentional misalignment from a pure-mode axis, and its magnitude and sign determine the extent of surface-wave diffraction. A later section will deal with these subjects in detail.

The fourth important material factor is temperature sensitivity as measured by the first order temperature coefficient of time delay. This quantity is given by

$$\frac{1}{\tau} \frac{\partial \tau}{\partial T} = \left( \frac{1}{v_s} \right)^{-1} \frac{\partial}{\partial T} \left( \frac{1}{v_s} \right) = \frac{1}{v_s} \frac{\partial}{\partial T} - \frac{1}{v_s} \frac{\partial v_s}{\partial T} = \alpha - \frac{1}{v_s} \frac{\partial v_s}{\partial T} \quad (11)$$

where  $1/v_s \partial v_s / \partial T$  is the velocity temperature coefficient,  $\tau = l/v_s$  is the delay time,  $l$  is the distance between two material points, and  $\alpha$  is the coefficient of thermal expansion. To calculate the temperature coefficient of time delay, the velocity temperature coefficient in equation (11) is approximated by

$$\frac{1}{v_s} \frac{\partial v_s}{\partial T} \approx \frac{1}{v_s(25^\circ\text{C})} \left[ \frac{v_s(35^\circ\text{C}) - v_s(15^\circ\text{C})}{20^\circ\text{C}} \right] \quad (12)$$

and the program described above is used to calculate SAW velocities at the various temperatures. Temperature sensitivity is important in many applications. For example, it has been shown that the principal limitation on the application of surface wave encoders and decoders to multiple-access secure communications systems is the degradation of the peak-to-sidelobe ratio of the autocorrelation function due to temperature differences (Carr, P.H., ... 1972). Also, in SAW bandpass filters the temperature stability of the center frequency is a direct function of the temperature coefficient of time delay of the substrate.

Since SAW materials are anisotropic, the four quantities discussed above are generally calculated for various crystalline orientations as continuous graphical functions of either direction of propagation in the plane of a plate (plates), as functions of the direction of the plate normal (boules), or for simultaneous rotation of both the plate normal and direction of propagation (cylinders). As an example, figure 5 shows plots of these four quantities as a function of the direction of propagation for the X cut of berlinite (Carr, P.H., ... 1976a). They were obtained by fixing the Euler angles  $\lambda$  and  $\mu$  at 90.0 degrees and varying the angle  $\theta$ .

## 3. PROPAGATION LOSS

The optimum design of a surface acoustic wave device requires an adequate knowledge of the many sources of overall device insertion loss. The relationship of insertion loss and fractional bandwidth to the piezoelectric coupling constant was discussed in the previous section. Other sources of device insertion loss include bidirectionality loss, electrical mismatch loss, parasitic transducer conduction loss, matching network loss, apodization loss, spurious mode generation loss, substrate propagation losses, and beam steering and diffraction. Discussions of the first six of these subjects can be found in references (IEEE Proceedings, 1976), (Hartmann, C.S., ... 1975), (IEEE Trans. MTT, 1973), and (Wagers, R.S., 1976).

Substrate propagation losses are considered in this section, and beam steering and diffraction will be discussed in the next section.

Total propagation loss is a superposition of three different mechanisms (Slobodnik, A.J., Jr., ... 1970): (1) Interaction with thermally excited elastic waves. (2) Scattering by crystalline defects and surface scratches. (3) Energy lost to air adjacent to the surface. The first mechanism is an inherent crystalline property, the magnitude of which can be predicted using viscosity theories (King, P.J., ... 1969). The second is, of course, highly undesirable and, fortunately, can be made negligible by proper crystal growth and polishing techniques (Slobodnik, A.J., Jr., ... 1970). The final mechanism is caused by the surface wave being phase matched to a longitudinal bulk wave in the air which results in a leaky-wave phenomenon. This so-called air loading can be eliminated by vacuum encapsulation or minimized by the use of a light gas (Slobodnik, A.J., Jr., 1972).

Propagation losses can be determined by directly probing the acoustic energy with a laser (Slobodnik, A.J., Jr., ... 1970). In this method, the surface wave deflects a small fraction of the incident light, which is detected with a photomultiplier tube and measured with a lock-in amplifier. The deflected light is directly proportional to the acoustic power of the surface wave.

Air loading can be determined by placing delay lines in a vacuum system and reducing the pressure below 1 torr while monitoring the change in insertion loss. Vacuum attenuation is, of course, the difference between the total propagation loss in air and the air loading component.

Frequency dependence of vacuum attenuation and air loading for three popular SAW substrates (Slobodnik, A.J., Jr., ... 1970), (Slobodnik, A.J., Jr., ... 1972), (Budreau, A.J., ... 1971), are illustrated in Figs. 6 and 7. Note the approximate  $f^2$  dependence of the vacuum attenuation and the linear dependence of the air loading. This allows an empirical expression for propagation loss to be derived from the data.

$$\text{Propagation Loss (dB/\mu s)} = (\text{VAC})F^2 + (\text{AIR})F \quad (13)$$

where  $F$  is in GHz. The coefficients VAC and AIR are tabulated for popular substrates in reference (Slobodnik, A.J., Jr., 1976). Equation (13) would be used, for example, when designing filters having particular band-pass characteristics.

#### 4. BEAM STEERING AND DIFFRACTION

##### 4.1 Parabolic Diffraction Theory

Diffraction of surface waves is a physical consequence of their propagation and can vary considerably depending upon the anisotropy of the substrate chosen. In fact, it is the slope of the power flow angle which determines the extent of both diffraction and beam steering (Szabo, T.L., ... 1973). There is an inherent tradeoff between these two important sources of loss.

A useful theory for calculating diffraction fields when the velocity anisotropy near pure-mode axes can be approximated by a parabola has been developed by Cohen (Cohen, M.G., 1967). By using a small angle approximation, he showed that for certain cases, the higher orders of the expression for the velocity could be neglected past the second order. That is,

$$\frac{v(\theta)}{v_0} \approx 1 + \frac{\gamma}{2} (\theta - \theta_0)^2 \quad (14)$$

where  $\gamma = \partial^2 v / \partial \theta^2$  and  $\theta_0$  is the angular orientation of the puremode axis. By comparing these approximations to an exact solution for electromagnetic diffraction in uniaxially anisotropic media, Cohen showed that the diffraction integral reduces to Fresnel's integral with the following change

$$\hat{z}' = \hat{z} | 1 + \gamma | \quad (15)$$

Szabo and Slobodnik (Szabo, T.L., ... 1973) introduced the absolute magnitude signs to account for those materials having  $\gamma < -1$  and the hatted terms to stand for wavelength scaled parameters ( $\hat{z} = z/\lambda$ ). In other words, diffraction is either accelerated or retarded depending on the value and sign of  $\gamma$ . Excellent agreement (Szabo, T.L., ... 1973) between this parabolic theory and experiment has been obtained whenever a good parabolic fit to the velocity is possible. In some cases, however, a more general theory is required.

##### 4.2 Angular Spectrum of Waves Diffraction Theory

In order to solve the most general homogeneous anisotropic problem, Kharusi and Farnell (Kharusi, M.S., ... 1971) applied the angular spectrum-of-waves technique to surface-wave diffraction. Their theory is valid for both the near and far fields, and for any direction including off-axis orientations. Its only limitation is the requirement of accurate knowledge of velocity values for the surface of interest. In implementing their theory the following integration is performed numerically for each field point:

$$A(X, Z) = \frac{1}{\pi} \int_{-\infty}^{\infty} \frac{\sin K_1 L / 2}{K_1} \cdot \exp j[(K_1 X + K_3(K_1) | Z |)] dK_1 \quad (16)$$

Here  $K_3$  and  $K_1$  are the projections of the wave-vector  $K$  along the  $Z$  and  $X$  axes, respectively, or in general, along directions perpendicular to and parallel to the transducer. The effect of introducing a laser probe in the profile measurements can be accommodated (Szabo, T.L., ... 1973) by inserting

$$\frac{\sin K_1 P / 2}{K_1 P / 2} \quad (17)$$

(in which  $P$  is the probe diameter) into the preceding integral (Eq. 16).

The real power of the exact anisotropic theory can be illustrated by its ability to predict even the fine structure of a diffraction pattern on a highly nonparabolic velocity surface, including profile asymmetry due to beam steering. An example is shown in Fig. 8. The case studied (Szabo, T.L., ... 1973) concerns

surface waves launched close to the 111-axis of 211-cut gallium arsenide at a frequency of 280 MHz. Transducer widths were  $\hat{L} = 51$ . This orientation was chosen (Szabo, T.L., ... 1973) because the velocity is non-parabolic and changes very rapidly with direction. The first column of Fig. 8 shows profiles for waves propagating exactly along the pure-mode 111-axis, a direction corresponding to  $\varphi = 0$ . Also note that the smoothing effect of the laser probe has not yet been included ( $\hat{P} = 0$ ). For the second column a misalignment of  $0.6^\circ$  from the 111-axis has been introduced, and the waves begin to take on the asymmetric behavior and beam steering of the experimental measurements (shown in the right-hand column) obtained using the laser probe (Slobodnik, A.J., Jr., ... 1970) technique. The third column introduces the same amount of angular misalignment as column two but, unlike the previous columns, includes the effect of a laser probe diameter of  $\hat{P} = 5.3$  wavelengths. The agreement between this column and the experimental curves is excellent.

#### 4.3 Quantitative Choice of Theory

The versatility of the exact angular spectrum of waves theory has been demonstrated; however, this approach is far more computationally complicated and costly than the parabolic theory. It also requires precise velocity surfaces as input data. Given a certain material, then, the designer must have guidelines from which he can choose the simplest appropriate theory.

The closeness of a given velocity surface to a parabolic curve can be determined by fitting the surface to a parabola and noting any deviation. In particular, second-order fits were obtained (Szabo, T.L., ... 1973) for various materials by using a least squares fit with relative velocity values computed to seven significant places within a range of  $\pm 5^\circ$  of  $(\theta - \theta_0) = 0$ . The maximum deviation of the fit from the velocity surface can be defined in terms of the quantity  $|\delta_M|$ . For comparative purposes, this deviation is expressed as a percentage of the actual velocity and, for convenience, is multiplied by a factor of  $10^5$ , i.e.,

$$|\delta_M| = \left| \frac{v_{\text{fit}} - v}{v} \right| \times 10^5. \quad (18)$$

A complete study of diffraction loss using the exact theory on many velocity surfaces not perfectly parabolic resulted in the following conclusion. Anisotropy may be conveniently grouped into two categories - parabolic ( $0 < |\delta_M| \lesssim 2.0$ ) and nonparabolic ( $2.0 \lesssim |\delta_M| < \infty$ ). Higher order terms discarded in the approximation of (Eq. 14) become significant (Szabo, T.L., ... 1973) for nonparabolic surfaces.

However for velocity surfaces having  $|\delta_M| \lesssim 2.0$ , the parabolic diffraction theory yields highly accurate results. Thus for all materials meeting this criterion, diffraction patterns are exactly equivalent in form, and merely scaled in distance by the factor  $|1 + \gamma|$  allowing universal diffraction loss curves to be calculated (Szabo, T.L., ... 1973). One such curve shown in Fig. 9 is a plot of diffraction loss versus the parameter  $(\hat{Z}/\hat{L}^2)|1 + \gamma|$ . This curve allows the determination of loss for any combination of transducer width and separation for all parabolic anisotropic velocity surfaces. It was calculated by integrating the complex acoustic amplitude over the aperture of the receiving transducer for identical unapodized input and output transducers (Szabo, T.L., ... 1973).

In the Fresnel region the loss never exceeds 1.6 dB, which is the loss at the far-field length,  $\hat{Z} = \hat{Z}_F$  (where the final peak in the beam profile has started its descent to a far-field pattern). The distance and transducer width at which a given loss will occur can always be given in far-field lengths. For example, the 3-dB loss point is

$$\hat{Z}_{3 \text{ dB}} = 1.769 \hat{Z}_F \quad (19)$$

where now

$$\hat{Z}_F = \frac{\hat{L}^2}{|1 + \gamma|}. \quad (20)$$

In the far field, the loss mechanism is the spreading of the beam with a slope of 10 dB/decade. The far-field loss can be approximated by

$$\text{Loss (dB)} = -10 \log \frac{\hat{Z}}{\hat{Z}_F}. \quad (21)$$

#### 4.4 Minimal Diffraction Cuts

One extremely important implication of the parabolic diffraction theory is that since it reduces to the isotropic theory scaled by the factor  $|1 + \gamma|$ , no diffraction spreading occurs for ideal parabolic surfaces having  $\gamma = -1$ . Material orientations approaching this ideal have, in fact, been discovered (Slobodnik, A.J., Jr., ... 1973b). A set of experimental SAW profiles for the 40.04 minimal diffraction cut (MDC) on bismuth germanium oxide are presented in Fig. 10. Experimentally, diffraction is suppressed by a factor of 100. These MDC orientations are allowing a new class of highly apodized acoustic surface-wave filters and long-time-delay devices to be realized.

#### 4.5 The Beam Steering Diffraction Tradeoff

As mentioned at the outset of this section, there is an inherent tradeoff between beam steering and diffraction. In anisotropic materials, beam steering occurs whenever transducers are misaligned from a pure-mode axis  $\theta_0$ , even though they may be perfectly aligned with each other. Beam steering is the pulling away of the acoustic beam from the transducer propagation axis by an additional angle,  $\varphi = \gamma(\theta - \theta_0)$ , as shown in Fig. 4. Let us discuss this tradeoff in more detail.

Diffraction is a fixed phenomenon for a given material, while beam steering can be controlled by precise X-ray alignment at the expense of increased device cost. Both, however, influence the choice of SAW substrate (Slobodnik, A.J., Jr., ... 1974). An example of how the combined loss of beam steering and diffraction varies among materials is illustrated (Slobodnik, A.J., Jr., ... 1974) in Fig. 11 where the loss is given as a function of  $\gamma$ .

For Fig. 11 the acoustic aperture is  $\hat{L} = 80$  wavelengths, the distance between input and output transducer is  $\hat{Z} = 5000$  wavelengths, and the misalignment from the desired pure-mode axis, or the beam steering (BS) angle, is  $BS \approx 0.1^\circ$ . In order to use these data for practical situations, it is only necessary to insert the slope of the power flow angle appropriate to the type and cut under consideration. It is also useful to note that  $\hat{Z} = tf$ ; where  $t$  is the time delay and  $f$  the frequency of the device of interest.

Several important features can be noted with reference to Fig. 11. Diffraction loss goes to 0 for those materials having  $\gamma = -1.0$  and, as expected, the combined loss curve agrees exactly with the beam steering loss curve. Those materials having  $\gamma = 0$  correspond to locally isotropic cases and beam steering goes to 0. Here, diffraction accounts for the total loss. Diffraction loss alone is symmetric about  $\gamma = -1.0$  and beam steering loss about  $\gamma = 0$ , while the combined curve is clearly nonsymmetric. Universal beam steering plus diffraction loss curves are not possible.

The results illustrated in Fig. 11 are of major importance in choosing a material for a particular application. For example, where diffraction is potentially a very serious problem, as in highly apodized filters, a material having  $\gamma = -1.0$  would be most desirable.

Figure 12 illustrates (Slobodnik, A.J., Jr., ... 1974) combined beam steering and diffraction loss versus the time-delay-frequency parameter  $\hat{Z}$ . It is of interest to point out that the loss is very high for the  $\hat{Z} = 75\,000$  curve near  $\gamma = -1.0$ . For this large distance beam steering is very important, especially for narrow undiffracted beams, and some beam spreading is to be desired. (The same is true if inaccurate X-ray orientation must be tolerated.) Since  $\hat{Z}$  is proportional to frequency (for fixed time delay), Fig. 12 also illustrates why beam steering and diffraction are considered UHF and microwave frequency design problems. Significant losses and material tradeoff considerations exist at the higher frequencies and, of course, also for very long time delays.

## 5. HIGH COUPLING, TEMPERATURE COMPENSATED MATERIALS

### 5.1 Introduction

A good deal of attention has recently been devoted to the development of SAW devices having broad bandwidth, low insertion loss, and temperature independent performance characteristics. As stated in the Introduction, neither quartz nor lithium niobate is adequate for such devices. This has resulted in a search for substrate materials that are temperature compensated and have piezoelectric coupling greater than that of ST cut quartz (Schulz, M.B., ... 1970). One material which has been extensively studied is lithium tantalate ( $\text{LiTaO}_3$ ). Although this material is temperature compensated for volume waves (Defaint, J., ... 1976), no temperature compensated cut is known to exist for surface acoustic waves. Nevertheless, as Fig. 1 shows, the piezoelectric coupling and temperature coefficient of time delay for lithium tantalate represent a reasonable compromise between the high coupling and poor temperature coefficient of lithium niobate and the very low coupling of temperature compensated quartz. Of particular interest is the minimum diffraction cut (MDC) of lithium tantalate, which has 1/20th the diffraction spreading of an isotropic material (Slobodnik, A.J., Jr., ... 1975). The  $\text{LiTaO}_3$  minimum diffraction cut has very low coupling to bulk waves, a very important property for low spurious response filters (Slobodnik, A.J., Jr., ... 1975) and delay lines (Carr, P.H., ... 1976b).

A major contribution to the search for improved materials has been the development of a phenomenological model (Newnham, R.E., 1973) which explains why known materials are temperature compensated. According to that model, temperature compensated materials possess either of the following anomalous properties: (1) a positive temperature coefficient of velocity or elastic constant or (2) a negative coefficient of thermal expansion. Quartz, for example, is temperature compensated because the temperature coefficient of  $C_{66}$ , the elastic constant for shear propagation along the Z axis, is positive (Newnham, R.E., 1973).

### 5.2 Berlinite

Berlinite, ( $\text{AlPO}_4$ ), is structurally similar to quartz with larger piezoelectric constants. A recent investigation (Chang, Z.P., ... 1976) has shown that for bulk waves berlinite is indeed temperature compensated along orientations similar to the AT and BT cuts of quartz, but with 2.5 times larger piezoelectric coupling. Motivated by these results for bulk waves and the fact that the temperature coefficient of one of berlinite's elastic constants is positive (Chang, Z.P., ... 1976). Studies have recently been conducted to investigate the behaviour of surface acoustic waves on berlinite (Carr, P.H., ... 1976a), (O'Connell, R.M., ... 1977a), (O'Connell, R.M., ... 1977b). That investigation has produced several temperature compensated cuts with more than four times the piezoelectric coupling of ST cut quartz (Carr, P.H., ... 1976a) (O'Connell, R.M., ... 1977a). High coupling, temperature compensated orientations have been found for doubly rotated cuts as well as for singly rotated cuts. In order to investigate the SAW behaviour of berlinite, the theoretical computer model described in Section 2 was used in conjunction with the data of reference (Chang, Z.P., ... 1976) to calculate the SAW velocity, the piezoelectric coupling, the electromechanical power flow angle, and the first order temperature coefficient of time delay for several standard crystallographic cuts (O'Connell, R.M., ... 1977b).

Results for the X cut of berlinite are shown in Figure 5. These and other initial results (Carr, P.H., ... 1976a) showed that berlinite is temperature compensated with four times the piezoelectric coupling of ST cut quartz. However, all of those initially reported cuts had non-zero electromechanical power flow angles, and consequently suffer from beam steering. Subsequent calculations produced two singly rotated cuts and two doubly rotated cuts, all of which have zero electromechanical power flow angles (O'Connell, R.M., ... 1977a). The most promising of the singly rotated cuts is the X axis boule  $80.4^\circ$  cut, a direct analog of the ST cut of quartz. The two cuts are compared in Table 1. Note that the piezoelectric coupling,  $\Delta V/V$ , of the X-axis boule  $80.4^\circ$  cut is more than four times as large as that of ST quartz, a distinct advantage. Other calculations have been made to investigate the behaviour of pseudo surface acoustic waves on berlinite (Jhunjunwala, A., ... 1976a).

Table 1 also shows that the slope of the power flow angle,  $\partial\phi/\partial\theta$ , is larger for the X axis boule  $80.4^\circ$  cut of berlinite than it is for the ST cut of quartz. According to the theory of SAW diffraction discussed in

Section 4, this means that ST cut quartz has better diffraction properties than the X axis boule 80.4° cut of berlinite. The desire to find temperature compensated cuts of berlinite having better diffraction properties than the singly rotated 80.4° cut motivated consideration of doubly rotated cuts. In particular, the  $\mu = 90.0$  plane of an orthogonal coordinate system having the three Euler angles  $\lambda$ ,  $\mu$ , and  $\theta$  as its basis was carefully searched. The  $\mu = 90.0$  plane was of particular interest because it contains four of the standard crystallographic cuts, including the X cut and Z axis cylinder, for which temperature compensated orientations were found earlier (Carr, P.H., ... 1976a).

The results are shown in Figure 13. The dashed and solid curves represent, respectively, the loci of Euler angles for which the electromechanical power flow angle and the temperature coefficient of time delay are zero. As can be seen in the blown up portion of the Figure, the loci intersect in a total of twelve places throughout the plane. Because of crystal symmetry, however, only two of the points are independent, and those circled in Figure 13 are listed in Table 1. Notice that while they have about the same piezoelectric coupling as the singly rotated 80.4° cut, the slopes of their power flow angles are smaller than those of either the 80.4° cut or the ST cut of quartz, giving them the added advantage of less diffraction spreading.

### 5.3 $\beta$ -Eucryptite

Another material which has been the subject of recent attention (Barsch, G.R., ... 1975) is  $\beta$ -eucryptite, (Li Al SiO<sub>4</sub>). This material is interesting because of its large negative coefficient of thermal expansion in the direction of the hexagonal C axis. According to the above-mentioned phenomenological model for explaining why certain materials are temperature compensated, this may give rise to temperature compensation even though the temperature coefficients of the elastic constants are all negative (Barsch, G.R., ... 1975). Using the theoretical computer model and data from references (Barsch, G.R., ... 1975), (Hummel, F.A., 1951), (Schulz, H., 1974), and (Bohm, H., 1975), calculations of the SAW properties of  $\beta$ -eucryptite produced both singly rotated and doubly rotated temperature compensated cuts. A singly rotated cut was found (O'Connell, R.M., ... 1977c) at X cut 69°, and is listed in Table 1 which shows that although the piezoelectric coupling for this cut is almost twice as large as that of ST quartz, it has the disadvantage of an 18 degree electromechanical power flow angle.

As was done in the case of berlinite, doubly rotated cuts were considered also, and a temperature compensated cut having a zero electromechanical power flow angle was found in the  $\lambda = 0.0^\circ$  plane (O'Connell, R.M., ... 1977c), as shown in Figure 14. As can be seen in the Figure, the loci intersect in a total of four places throughout the plane. Again, because of crystal symmetry, only one of the points is independent, and it is listed in Table 1 where it can be seen that, unfortunately, the piezoelectric coupling of this doubly rotated cut is only about half as large as that of ST quartz. Perhaps the most attractive feature of this material is that it has the highest SAW velocity of all the temperature compensated materials listed in Table 1, 3662 m/sec.

### 5.4 Other Temperature Compensated Materials

The sulfosalts are a class of materials of the form  $Tl_3BX_4$ , where B can be V, Nb, or Ta, and X can be S or Se. Recent calculations have shown that at least two of these materials are temperature compensated with significantly larger piezoelectric coupling than berlinite (Weinert, R.W., ... 1975), (Isaacs, T.J., ... 1976). One particular cut of  $Tl_3VS_4$ , for example, has four times the piezoelectric coupling of berlinite (Weinert, R.W., ... 1975). As shown in Table 1, however, this cut has the disadvantage of a rather large electromechanical power flow angle, about -17 degrees. Another cut of the same material and one of  $Tl_3TaSe_4$ , having zero electromechanical power flow angles, have also been found (Jhunjhunwala, A., ... 1976b). As the data in Table 1 shows, the piezoelectric coupling of these cuts is not as large as that of the first cut discussed, but it is still more than twice as large as that of berlinite. The table also shows that the SAW velocities of the sulfosalts are only about 1/3 as large as that of berlinite. This is a disadvantage for high frequency applications, but an advantage for long delay lines and low frequency SAW filters.

A composite material, consisting of a film of silicon dioxide on lithium tantalate, has also been shown to be temperature compensated (Parker, T.E., ... 1975). This material has, as shown in Table 1, a very small electromechanical power flow angle, a piezoelectric coupling of about .007, and a relatively large SAW velocity. The most attractive feature of the material is that its second order temperature coefficient of time delay is nearly an order of magnitude smaller than that of ST cut quartz. Despite these positive attributes, the composite has several drawbacks due to the SiO<sub>2</sub> film, including: (1) its thickness must be very accurately controlled, (2) it is very lossy at high frequencies, and (3) it is dispersive.

Besides those materials which have been shown to be temperature compensated, there are several others which, for various reasons, may prove to be. For example, nepheline, (KAlSi<sub>3</sub>O<sub>8</sub>) (NaAlSi<sub>3</sub>O<sub>8</sub>), should have temperature compensated orientations because the temperature coefficients of the elastic constants  $C_{11}$  and  $C_{66}$  are positive (Bonczar, L.J., ... 1975). Also, lead potassium niobate (Pb<sub>2</sub>KNb<sub>2</sub>O<sub>7</sub>), which has piezoelectric coupling factors of the order 0.7 for bulk waves, shows promise of being temperature compensated because it possesses opposite signs for the temperature coefficients of the bulk wave resonance frequency for different vibrational modes (Barsch, G.R., ... 1976).

## 6. FAST VELOCITY MATERIALS

Fast velocity materials, such as beryllium oxide and aluminum nitride, are of great interest for extending the upper frequency limit of SAW devices. Also, the high thermal conductivity of these materials results in a high power handling capacity; for example, continuous wave power levels of 1W produced no damage to a transducer operating at 1 GHz (Budreau, A.J., ... 1974a). Beryllium oxide single crystals have been grown in centimeter sizes (Hagon, P.J., ... 1971). The velocity of surface acoustic waves is 6500 m/sec. The very weak piezoelectric coupling (1/10th that of quartz) and the strong coupling to volume waves make this material unattractive compared to aluminum nitride thin-films-on-sapphire, which have unusually low coupling to volume waves and a piezoelectric coupling up to six times that of ST-quartz. The velocity of the films varies from about 6000 m/sec for very thin films to 5500 m/sec for 0.7 wavelength thick films (Liu, J.K., ... 1975a). Also their temperature coefficients vary from 47 ppm for a very thin film to 25 ppm for

a film 0.57 wavelengths thick (Liu, J.K., ... 1975b). Single crystals of aluminum nitride have been grown in sizes up to only several millimeters (Dugger, C.O., 1974). (Slack, G.A., ... 1976); larger crystals are needed for measuring the unknown elastic constants.

Velocity nonuniformities from one side to the other of a 1 cm wide sample have been observed to be of the order of 0.5% for thin films of AlN grown on sapphire by chemical vapor deposition (Budreau, A.J., ... 1974b). This velocity difference is of course most critical for narrowband SAW filter applications. Another problem has been the lack of reproducibility of the piezoelectric coupling from sample to sample. Liu, et. al. (Liu, J.K., ... 1975a), (Liu, J.K., ... 1975b) have shown that this can be due to misalignment of the pyramidal grains of the as-grown thin films. The granularity is so severe that the films must first be polished to avoid scattering the surface acoustic waves. Initial results with films grown by reactive rf sputtering show that they do not have this granularity; thus, this method of growing films warrants further investigation (Shuskus, A.J., ... 1974).

## 7. CONCLUSIONS

Clearly, the task of choosing a substrate material for a SAW device is not trivial. There are many factors which must be considered, most of which have been discussed here. Fortunately, the relative importance of these factors varies with the specific device and application at hand. It is hoped that the topics discussed herein will provide the design engineer with a reasonable understanding of the many factors involved in SAW device substrate choice, and with a useful set of guidelines for weighing the relative importance of those factors in a specific design.

## REFERENCES

- BARSCH, G. R. AND SPEAR, K.E., 1975, "Temperature Compensated Piezoelectric Materials," AFRL Report No. TR-75-0609, Contract No. F19628-75-C-0085.
- BARSCH, G.R. AND SPEAR, K.E., 1976, "Temperature Compensated Piezoelectric Materials," RADC Report No. TR-76-184, Contract No. F19628-75-C-0085.
- BOHM, H., 1975, "Dielectric Properties of  $\beta$ -Eucryptite," Phys.Stat.Sol., Vol. (a) 30, p 531.
- BONCZAR, L.J., AND BARSCH, G.R., 1975, "Elastic and Thermoelastic Constants of Nepheline," J.Appl.Phys., vol 46, pp 4339-4340.
- BUDREAU, A.J. AND CARR, P.H., 1971, "Temperature Dependence of the Attenuation of Microwave Frequency Elastic Surface Waves in Quartz," J.Appl.Phys., vol. 18, pp. 239-241.
- BUDREAU, A.J., SILVA, J.H., AND LAKER, K.R., 1974a "Microwave Frequency SAW Filters on Aluminum Nitride-on-Sapphire and Beryllium Oxide," 1974 Ultrasonics Symp. Proc. IEEE Cat No 74896-1SU, p 299.
- BUDREAU, A.J., LAKER, K.R., AND CARR, P.H., 1974b, "Compact Microwave Acoustic Surface Wave Filter Bank for Frequency Synthesis," Proceedings of the Symposium on Optical and Acoustical Micro-Electronics, Polytechnic Institute of New York, p 471.
- BUDREAU, A.J., KEARNS, W.J., AND CARR, P.H., 1975, "State-of-the-art in Microfabrication of SAW Devices," 1975 Ultrasonics Symposium Proceedings, IEEE Cat. No. 75 CHO 994-4SU, pp 458-462.
- CAMPBELL, J.J. AND JONES, W.R., 1968, "A Method for Estimating Optimal Crystal Cuts and Propagation Directions for Excitation of Piezoelectric Surface Waves," IEEE Trans. Sonics Ultrason., vol. SU-15, pp. 209-218.
- CARR, P.H., DeVITO, P.A., AND SZABO, T.L., 1972, "The Effect of Temperature and Doppler Shift on the Performance of Elastic Surface Wave Encoders and Decoders," IEEE Trans.Sonics Ultrason., vol.SU-19, pp. 357-367.
- CARR, P.H. AND O'CONNELL, R.M., 1976a, "New Temperature Compensated Materials with High Piezoelectric Coupling," Proc. of the 30th Annual Symposium on Frequency Control, pp 129-131.
- CARR, P.H., FENSTERMACHER, T.E., SILVA, J.H., KEARNS, W.J., AND STIGLITZ, M.R., 1976b, "SAW Delay Line With All Spurious 70 dB Down," 1976 Ultrasonics Symposium Proceedings, IEEE Cat.No. 76 CH120-5SU, p 459.
- CHANG, Z.P. AND BARSCH, G.R., 1976, "Elastic Constants and Thermal Expansion of Berlinite," IEEE Trans.on Sonics and Ultrasonics, Vol. SU-23, pp 127-135.
- COHEN, M.G., 1967, "Optical Study of Ultrasonic Diffraction and Focussing in Anisotropic Media," J.Appl. Phys., vol. 38, pp 3821-3828.
- COLLINS, J.H., GERARD, H.M., AND SHAW, H.J., 1968, "High-Performance Lithium Niobate Acoustic Surface Wave Transducers and Delay Lines," Appl.Phys.Lett., vol. 13, pp. 312-313.
- COQUIN, G.A. AND TIERSTEN, H.F., 1967, "Analysis of the Excitation and Detection of Piezoelectric Surface Waves in Quartz by Means of Surface Electrodes," J.Acoust.Soc.Amer., vol. 41, pp. 921-939.
- DETAINT, J. AND LANCON, R., 1976, "Temperature Characteristics of High Frequency Lithium Tantalate Plates," Proc. of the 30th Annual Symposium on Frequency Control, p 132.
- DUGGER, C. O., 1974, "The Synthesis of Aluminum Nitride Single Crystals," Mat.Res.Bull., vol 9; p 331.
- GOLDSTEIN, H., 1950, Classical Mechanics, Reading, MA: Addison-Wesley.

- HAGON, P.J. AND AUSTERMAN, S.B., 1971, "Acoustic Waves in Beryllium Oxide Crystal," *Appl. Phys. Letters*, Vol 18, p 102.
- HARTMANN, C.S., BELL, D.T., JR., AND ROSENFELD, R.C., 1975, "Impulse Model Design of Acoustic Surface-Wave Filters," *IEEE Trans. Microwave Theory Tech.*, Vol. MTT-21, pp 162-175.
- HAYS, R.M., AND HARTMANN, C.S., 1976, "Surface-Acoustic-Wave Devices for Communications," *Proc. IEEE*, Vol 64, pp 652-671.
- HUMMEL, F.A., 1951, "Thermal Expansion Properties of Some Synthetic Lithia Minerals," *J. Am. Ceram. Soc.*, Vol 34, p 235.
- IEEE Proceedings, 1976, "Special Issue on Surface Acoustic Waves," Vol 64, No. 5.
- IEEE Trans. Microwave Theory Tech., 1973, Special Issue on Microwave Acoustic Signal Processing, Vol MTT-21, No. 4.
- INGEBRIGTSEN, K.A., 1969, "Surface Waves In Piezoelectrics," *J. Appl. Phys.*, vol. 40, pp 2681-2686.
- ISAACS, T.J., AND WEINERT, R.W., 1976, "Crystal Growth and Properties of  $\text{Ti}_3\text{BX}_4$  Crystals for Acoustic Surface-Wave and Bulk Acoustic Devices," *Journal of Electronics Materials*, Vol 5, pp 13-22.
- JHUNJHUNWALA, A., VETELINO, J.F., AND FIELD, J.C., 1976a, "Berlinite, A Temperature Compensated Material for Surface Acoustic Wave Applications," *Proc. of the 1976 Ultrasonics Symposium*, pp. 523-527.
- JHUNJHUNWALA, A., VETELINO, J.F., AND FIELD, J.C., 1976b, "Temperature Compensated Cuts with Zero Power Flow in  $\text{Ti}_3\text{VS}_4$  and  $\text{Ti}_3\text{TaSe}_4$ ," *Electronics Letters*, Vol. 12, pp 683-684.
- JONES, W.R., CAMPBELL, J.J., AND VEILLEUX, S.L., 1969, "Theoretical Analysis of Acoustic Surface Waves," Hughes Aircraft Co., Fullerton, CA, Final Report F19628-69-0132, unpublished.
- KHARUSI, M.S. AND FARNELL, G.W., 1971, "Diffraction and Beam Steering for Surface-Wave Comb Structures on Anisotropic Substrates," *IEEE Trans. Sonics Ultrason.*, vol. SU-18, pp. 35-42.
- KING, P.J. AND SHEARD, F.W., 1969, "Viscosity Tensor Approach to the Damping of Rayleigh Waves," *J. Appl. Phys.*, vol. 40, pp. 5189-5190.
- LIU, J.K., LAKIN, K.M., AND WANG, K.L., 1975a, "Growth Morphology and SAW Measurements of AlN Films on Sapphire," *J. Appl. Phys.*, vol 46, p 3703.
- LIU, J.K., STOKES, R.B., AND LAKIN, K.M., 1975b, "Evaluation of AlN Films on Sapphire for SAW Applications," 1975 Ultrasonics Symposium Proceedings, IEEE Cat. No. CH0 994-4SU, p 234.
- NEWMHAM R.E., 1973, "Elastic Properties of Oxides and the Search for Temperature Compensated Materials," AFRL Report No. TR-73-0220, Contract No. F19628-73-C-0108.
- O'CONNELL, R.M., AND CARR, P.H., 1977a, "High Piezoelectric Coupling, Temperature Compensated Cuts of Berlinite,  $\text{AlPO}_4$ , for SAW Applications," *IEEE Trans. on Sonics and Ultrasonics*.
- O'CONNELL, R.M., AND CARR, P.H., 1977b, "New Materials for Surface Acoustic Wave (SAW) Devices," *Optical Engineering*.
- O'CONNELL, R.M. AND CARR, P.H., 1977c, "Temperature Compensated Cuts of Berlinite and  $\beta$ -eucryptite for SAW Devices," 31st Annual Frequency Control Proceedings (to be published).
- PARKER, T.E. AND SHULZ, M.B., 1975, "Stability of SAW Controlled Oscillators," *Proc. of the 1975 Ultrasonics Symposium*, pp 261-263.
- RAYLEIGH, LORD, 1885, "On Waves Propagated Along the Plane Surface of an Elastic Solid," *Proc. London Math. Soc.*, vol 17, pp. 4-11.
- SCHULZ, H., 1974, "Thermal Expansion of Beta Eucryptite," *J. Am. Ceram. Soc.*, Vol 57, p 313.
- SCHULZ, M.B., MATSINGER, B.J., AND HOLLAND, M.G., 1970, "Temperature Dependence of Surface Acoustic Wave Velocity on  $\alpha$  Quartz," *J. Appl. Phys.*, Vol 41, pp 2755-2765.
- SCHULZ, M.B. AND MATSINGER, J.H., 1972, "Rayleigh-wave Electromechanical Coupling Constants," *Appl. Phys. Lett.*, vol. 20, pp 367-369.
- SHUSKUS, A.J., REEDER, T.M., AND PARADIS, E.L., 1974, "RF-Sputtered Aluminum Nitride Films on Sapphire," *Appl. Phys. Letters*, vol 24, p 155.
- SLACK, G.A. AND McNELLY, T.R., 1976, "Growth of High Purity AlN Crystals," *J. of Crystal Growth*, Vol 34, p 263.
- SLOBODNIK, A.J., JR., CARR, P.H., AND BUDREAU, A.J., 1970, "Microwave Frequency Acoustic Surface-Wave Loss Mechanisms on  $\text{LiNbO}_3$ ," *J. Appl. Phys.*, vol 41, pp 4380-4387.
- SLOBODNIK, A. J., JR., 1972, "Attenuation of Microwave Acoustic Surface Waves Due to Gas Loading," *J. Appl. Phys.*, vol. 43, pp 2565-2568.
- SLOBODNIK, A.J., JR., AND BUDREAU, A.J., 1972, "Acoustic Surface Wave Loss Mechanisms on  $\text{Bi}_{12}\text{GeO}_{20}$  at

2-1-10

Microwave Frequencies," J. Appl. Phys., vol. 43, pp 3278-3283.

SLOBODNIK, A.J., JR., CONWAY E.D., AND DELMONICO, R.T., 1973a, "Microwave Acoustics Handbook, Vol. 1A, Surface Wave Velocities," AFCRL, Hanscom AFB, MA 01731, TR-73-0597, unpublished.

SLOBODNIK, A.J., JR., SZABO, T.L., 1973b, "Minimal Diffraction Cuts for Acoustic Surface Wave Propagation on  $\text{Bi}_{12}\text{GeO}_{20}$ ," J. Appl. Phys., vol. 44, pp 2937-2941.

SLOBODNIK, A.J., JR., SZABO, T.L., 1974, "Design of Optimum Acoustic Surface Wave Delay Lines at Microwave Frequencies," IEEE Trans. Microwave Theory Tech., vol. MMT-22, pp 458-462.

SLOBODNIK, A.J., JR., FENSTERMACHER, T.E., KEARNS, W.J., ROBERTS, G.A., AND SILVA, J.H., 1975, "A Minimal Diffraction Lithium Tantalate Substrate for Contiguous SAW Butterworth Filters," 1975 Ultrasonics Symposium Proceedings, IEEE Cat. No. 75 CHO 994-4SU, p 405.

SLOBODNIK, A.J., JR., 1976, "Surface Acoustic Waves and SAW Materials," Proc. IEEE, Vol 64, pp 581-595.

SZABO, T.L. AND SLOBODNIK, A.J., JR., 1973, "The Effect of Diffraction on the Design of Acoustic Surface Wave Devices," IEEE Trans. Sonics Ultrason., vol. SU-20, pp 240-251.

TIERSTEN, H.F., 1963, "Thickness Vibrations of Piezoelectric Plates," J. Acoust. Soc. Amer., vol. 35, pp 53-58.

WEINERT, R.W. AND ISAACS, T.J., 1975, "New Piezoelectric Materials Which Exhibit Temperature Stability for Surface Waves," Proc. of the 29th Annual Symposium on Frequency Control, pp 139-142.

WHITE, R.M. AND VOLTHER, F.W., 1965, "Direct Piezoelectric Coupling to Surface Elastic Waves," Appl. Phys. Lett., vol. 7, pp. 314-316.

WAGERS, R.S., 1976, "Spurious Acoustic Responses in SAW Devices," Proc. IEEE, Vol. 64, pp 699-702.

## FIGURES

- Figure 1      Temperature coefficient of time delay versus piezoelectric coupling for various SAW materials.
- Figure 2.      Schematic representation of the generation and propagation of a surface acoustic wave.
- Figure 3.      Illustration of the coordinate system used to define SAW propagation. The shorting plane will be necessary when computing the quantity  $\Delta v/v$ .
- Figure 4.      Schematic representation of the profiles of a propagating acoustic surface wave on a crystalline substrate. Angle  $\theta$  defines direction of propagation with respect to reference crystalline axis, and angle  $\phi$  defines deviation of power flow from phase velocity direction.
- Figure 5.      The variation of (a) SAW velocity (b) piezoelectric coupling (c) power flow angle, and (d) temperature coefficient of time delay for X-cut Berlinite.
- Figure 6.      SAW attenuation in vacuum as a function of frequency for YZ  $\text{LiNbO}_3$ , 001, 110 and 111, 110,  $\text{Bi}_{12}\text{GeO}_{20}$ , and YX quartz. Experimental slopes are all approximately  $f^2$ .
- Figure 7.      SAW attenuation due to air loading as a function of frequency for materials listed in Figure 6. It is interesting to note nearly identical results for  $\text{LiNbO}_3$  and  $\text{Bi}_{12}\text{GeO}_{20}$ .
- Figure 8.      Theoretical and experimental surface-wave profiles illustrating diffraction near 111-axis of 211-cut gallium arsenide.  $\hat{z}$  indicates distance for propagation in wavelengths from input transducer,  $\theta$  gives the misorientation from 111-axis, and  $\hat{P}$  is laser probe diameter in acoustic wavelengths.

- Figure 9. Universal diffraction loss curve for all parabolic materials as a function of  $(\hat{Z}/\hat{L}^2) |1 + \gamma|$ . To convert to the actual distance in wavelengths on horizontal scale simply insert  $\hat{L}$ , width of your transducer in wavelengths, and  $\gamma$  appropriate to your material.
- Figure 10. Illustration of the two orders of magnitude diffraction suppression achieved using the 40.04  $\text{Bi}_{12}\text{GeO}_{20}$  minimal diffraction cut. An acoustic aperture of  $\hat{L} = 40.56$  wavelengths was used.
- Figure 11. Loss due to diffraction and beam steering as a function of slope of power flow angle for parabolic materials.  $\hat{L}$  represents width of transducer in wavelengths,  $\hat{Z}$  the distance between transducers in wavelengths, and BS  $\Delta$  the beam steering angle (defined as misalignment of center line between transducers from desired pure-mode axis).
- Figure 12. Loss due to diffraction and beam steering as a function of slope of power flow angle with distance in wavelengths between transducers,  $\hat{Z}$  as parameter.
- Figure 13. Loci of Euler angles having zero electromechanical power flow angle (dashed lines) and zero temperature coefficient of time delay (solid lines) in the  $\mu = 90.0$  plane of berlinite.
- Figure 14. Loci of Euler angles having zero electromechanical power flow angle (dashed lines) and zero temperature coefficient of time delay (solid lines) in the  $\lambda = 0.0$  plane of  $\beta$ -eucryptite.

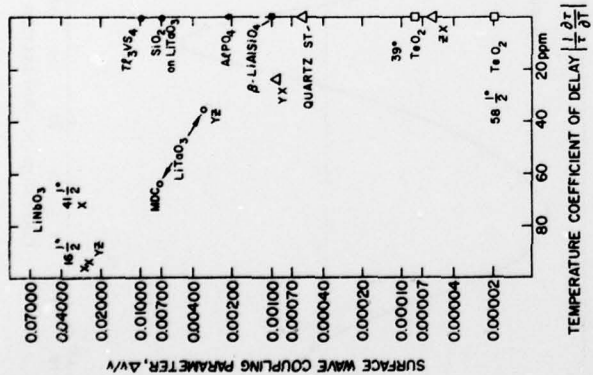


TABLE I. TEMPERATURE COMPENSATED CUTS OF VARIOUS MATERIALS

| MATERIAL  | ORIENTATION        | EULER ANGLES<br>$\chi$ | POWER FLOW<br>ANGLE $\theta$ (DEG) | SLOPE OF<br>SCATTERING<br>ANGLE $\phi$ (DEG) | $\Delta n$<br>VELOCITY<br>( $\times 10^{-2}$ ) |
|---|--------------------|------------------------|------------------------------------|--|--|
| QUARTZ<br>(SiO <sub>2</sub> )                           | 5° CUT             | 0 132 75 0             | 0.0                                | 0.378  | 3158   |
| BELLENITE<br>(AlPO <sub>4</sub> )                       | X AXIS BOULE 80.4° | 0 80.4 0               | 0.0                                | 0.901  | 2751   |
|   | DOUBLY ROTATED, A  | 76.8 90 11.5           | 0.0                                | 0.372  | 2756   |
|   | DOUBLY ROTATED, B  | 79.7 90 15.5           | 0.0                                | 0.221  | 2758   |
| B-EUCRYPTITE<br>(BaLiAlSi <sub>3</sub> O <sub>9</sub> ) | X CUT 69°          | 90 90 69               | 18                                 | --   | 3662   |
|   | DOUBLY ROTATED     | 0 57 62                | 0.0                                | 0.32   | 3258   |
| Ti <sub>3</sub> Al <sub>3</sub>                         | (110) CUT 70°      | -45 90 70              | -17                                | --   | 900  |
|   | (110) CYLINDER 24° | 45 24 90               | 0.0                                | --   | 1010   |
|   | (110) CYLINDER 54° | 45 54 90               | 0.0                                | --   | 979  |
| SiO <sub>2</sub> -Li <sub>2</sub> SiO <sub>3</sub>      | Y CUT, Z GROUP     | 0 90 90                | 0.0                                | --   | 3945   |

Figure 2

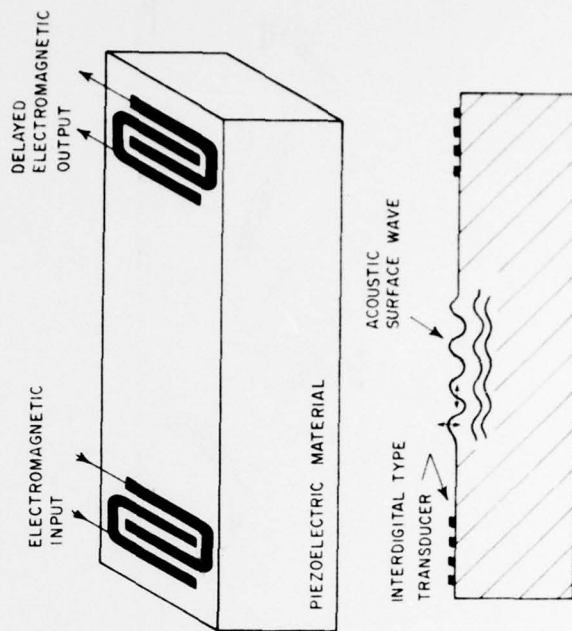


Figure 3.

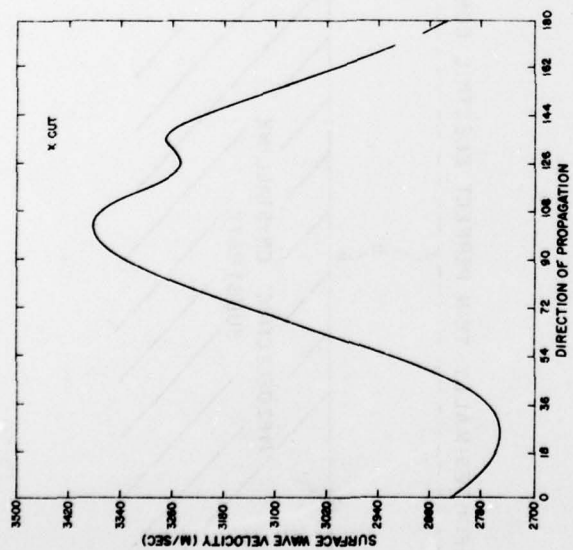


Figure 5A

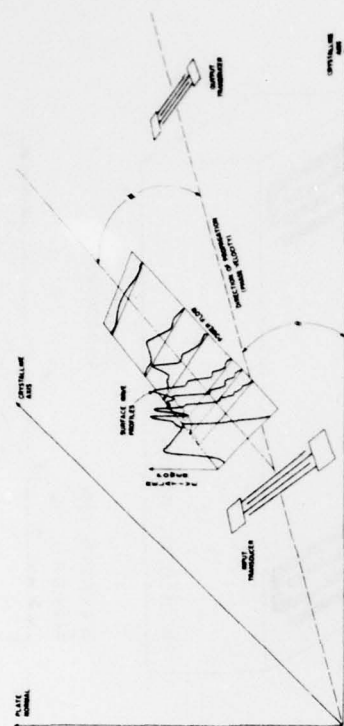


Figure 4

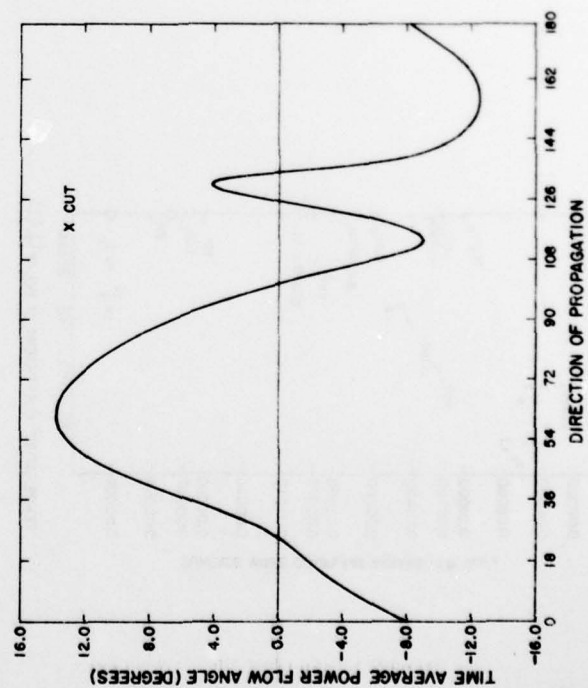


Figure 5C

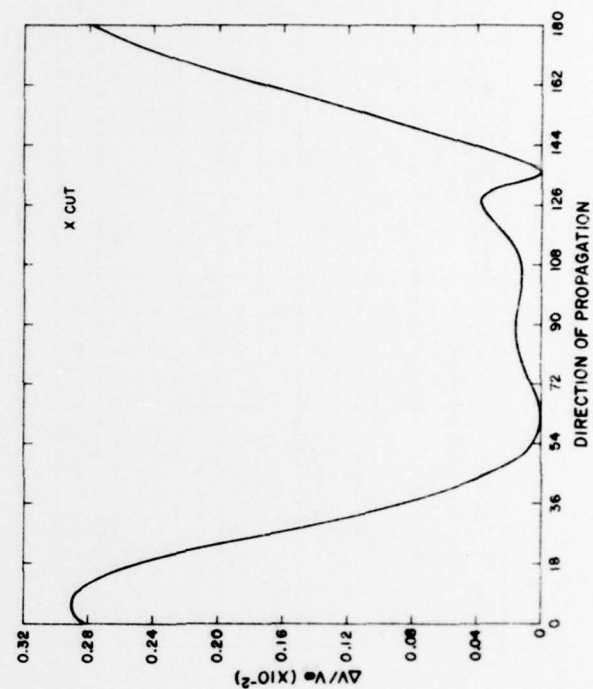


Figure 5B

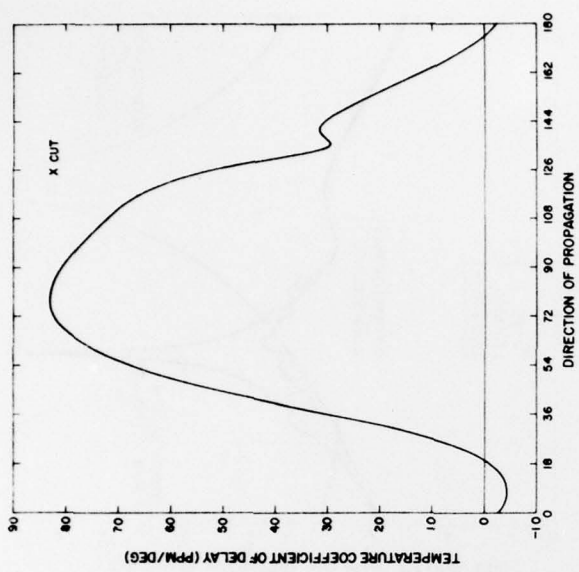


Figure 50

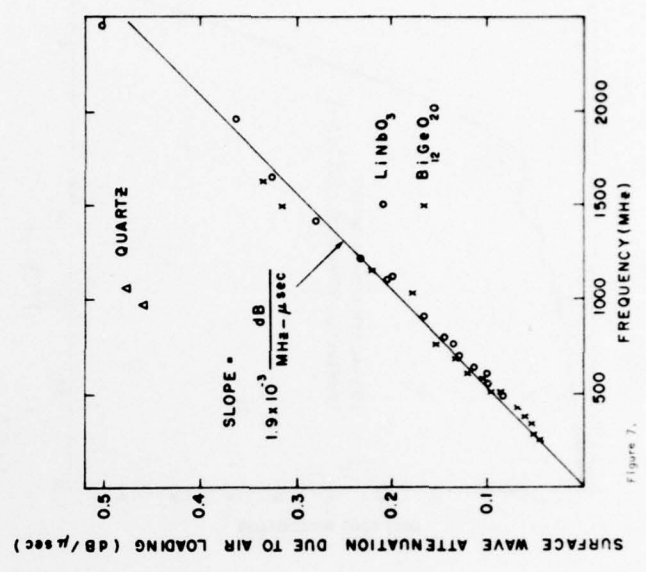


Figure 7.

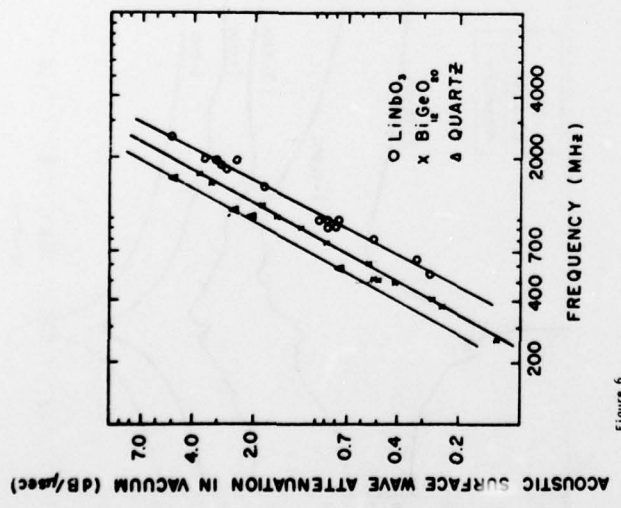


Figure 6.

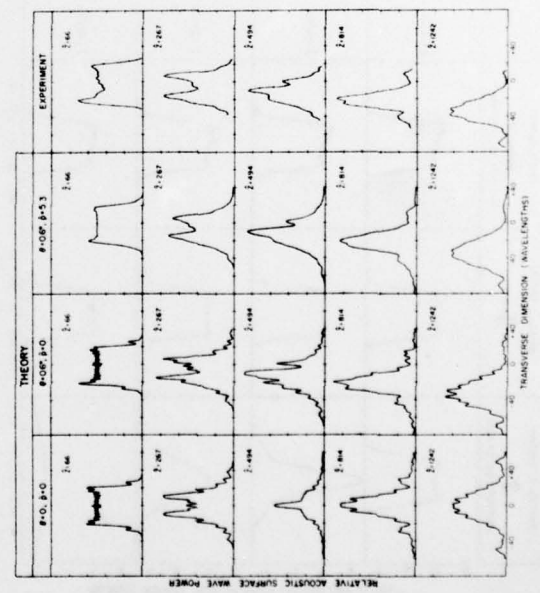


Figure 8.

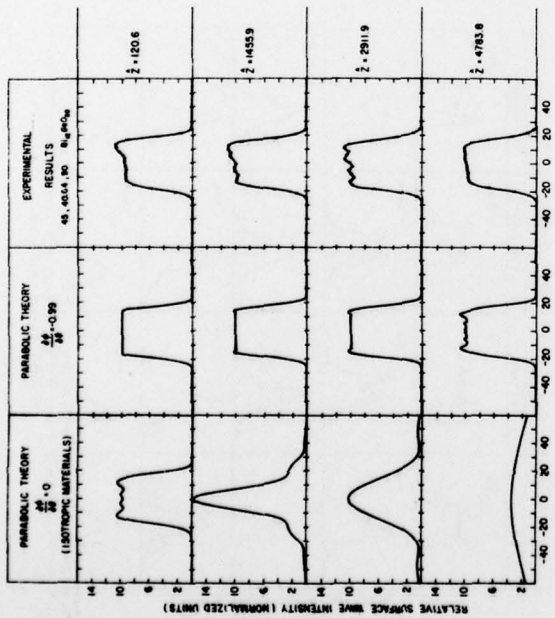


Figure 10.

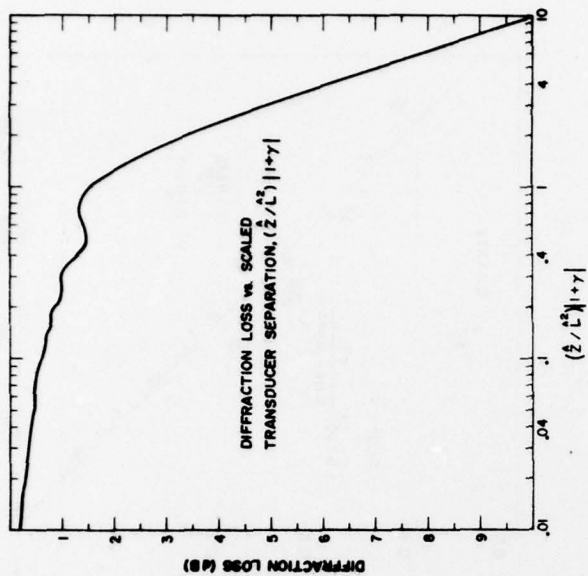


Figure 9.

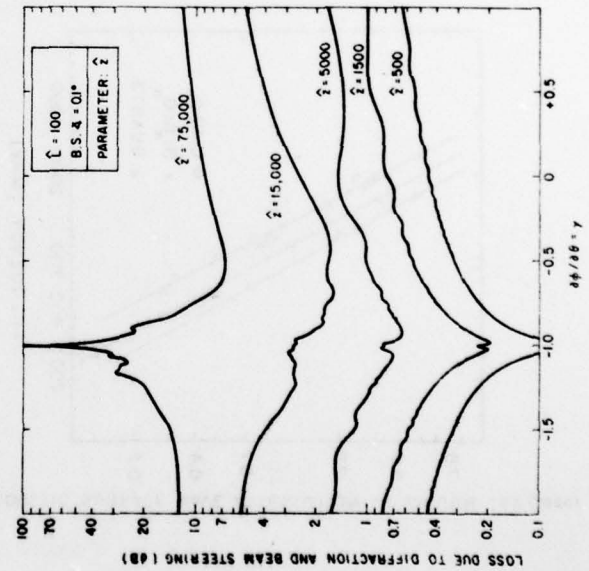


Figure 12.

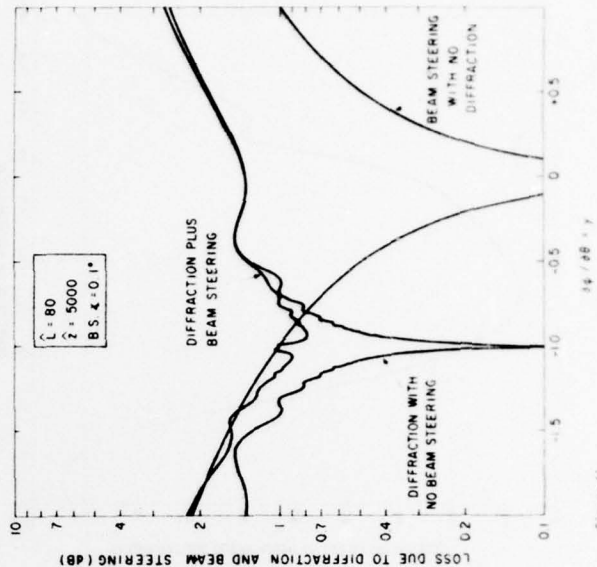


Figure 11.

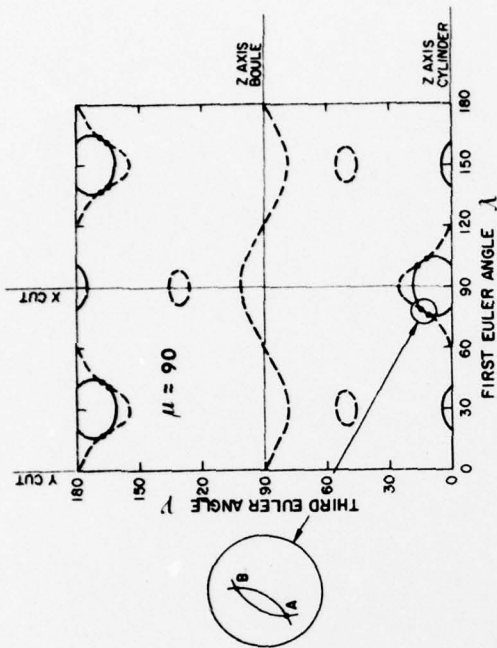
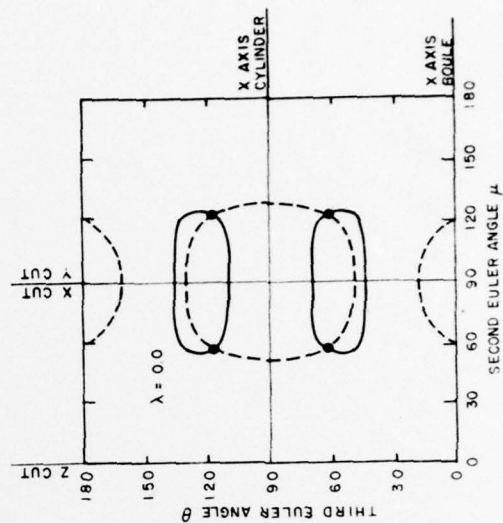


Figure 13.



DDC  
 RECEIVED  
 NOV 28 1977  
 RECEIVED  
 A

|                                      |   |
|--------------------------------------|---|
| ACCESSION FOR                        |   |
| NTIS                                 | White Section <input checked="" type="checkbox"/> |
| DOC                                  | Self Section <input type="checkbox"/>             |
| UNANNOUNCED <input type="checkbox"/> |   |
| JUSTIFICATION                        |   |
| BY                                   |   |
| DISTRIBUTION/AVAILABILITY CODES      |   |
| DIR.                                 | AVAIL. AND/OR SPECIAL                             |
| A                                    |   |

| REPORT DOCUMENTATION PAGE  |                       | READ INSTRUCTIONS<br>BEFORE COMPLETING FORM  |
|--|-----------------------|--|
| 1. REPORT NUMBER<br><b>ETR-77-0034</b>   | 2. GOVT ACCESSION NO. | 3. RECIPIENT'S CATALOG NUMBER  |
| 4. TITLE (and Subtitle)<br><b>MATERIAL CHOICE FOR OPTIMUM SAW DEVICE PERFORMANCE</b>   |                       | 5. TYPE OF REPORT & PERIOD COVERED<br><b>Scientific Interim</b>                              |
|  |                       | 6. PERFORMING ORG. REPORT NUMBER   |
| 7. AUTHOR(s)<br><b>R. M. O'Connell<br/>A. J. Slobodnik, Jr.<br/>P. H. Carr</b>   |                       | 8. CONTRACT OR GRANT NUMBER(s)   |
| 9. PERFORMING ORGANIZATION NAME AND ADDRESS<br><b>Deputy for Electronic Technology (RADC/EEA)<br/>Hanscom AFB<br/>Massachusetts 01731</b>  |                       | 10. PROGRAM ELEMENT, PROJECT, TASK<br>AREA & WORK UNIT NUMBERS<br><b>61102F<br/>2305J501</b> |
| 11. CONTROLLING OFFICE NAME AND ADDRESS<br><b>Deputy for Electronic Technology (RADC/EEA)<br/>Hanscom AFB<br/>Massachusetts 01371</b>  |                       | 12. REPORT DATE<br><b>22 November 1977</b>   |
|  |                       | 13. NUMBER OF PAGES<br><b>17</b>   |
| 14. MONITORING AGENCY NAME & ADDRESS (if different from Controlling Office)  |                       | 15. SECURITY CLASS. (of this report)<br><b>Unclassified</b>                                  |
|  |                       | 15a. DECLASSIFICATION DOWNGRADING<br>SCHEDULE  |
| 16. DISTRIBUTION STATEMENT (of this Report)<br><b>Approved for public release; distribution unlimited.</b>   |                       |  |
| 17. DISTRIBUTION STATEMENT (of the abstract entered in Block 20, if different from Report)   |                       |  |
| 18. SUPPLEMENTARY NOTES<br><b>Published in the NATO-AGARD Conference Proceedings, Ottawa, Canada,<br/>11-15 October 1977. AGARD Conference Preprint No. 230, <u>Impact of Charge Coupled<br/>Devices and Surface Acoustic Wave Devices on Signal Processing and Imagery in<br/>Advanced Systems</u></b>  |                       |  |
| 19. KEY WORDS (Continue on reverse side if necessary and identify by block number)<br><b>Surface Acoustic Waves (SAW)<br/>Temperature Compensated Materials<br/>Material Design Parameters<br/>Optimum SAW Substrates</b>  |                       |  |
| 20. ABSTRACT (Continue on reverse side if necessary and identify by block number)<br><b>The theory of surface acoustic wave propagation is reviewed and some of the<br/>various material design parameters which follow from the theory and which must<br/>be considered in making the optimum SAW device substrate choice are discussed.<br/>The parameters covered include SAW velocity, piezoelectric coupling constant,<br/>electromechanical power flow angle, temperature sensitivity, propagation losses,<br/>and beam steering and diffraction. Depending upon the device being designed and<br/>the application, some of these parameters are more important than others. In the<br/>design of temperature stable, broadband, low insertion loss devices, the import-</b> |                       |  |

DD FORM 1473

EDITION OF 1 NOV 65 IS OBSOLETE

Unclassified

SECURITY CLASSIFICATION OF THIS PAGE (When Data Entered)

ant requirements are a zero temperature coefficient of time delay and a large piezoelectric coupling constant. Alternatively, the design of high frequency devices requires low loss substrate materials with large SAW velocities. The state-of-the-art in the development of new materials for these two classes of devices is reviewed.

↑

Unclassified

ATE  
LMED  
-8